ACS OMEGA

http://pubs.acs.org/journal/acsodf

Article

Lattice Resonances Excited by Finite-Width Light Beams

Lauren Zundel,[§] Juan R. Deop-Ruano,[§] Rosario Martinez-Herrero, and Alejandro Manjavacas*

Cite This: https://doi.org/10.1021/acsomega.2c03847

Read Online

ACCESS | Metrics & More | Article Recommendations | Supporting Information

ABSTRACT: Periodic arrays of metallic nanostructures support collective lattice resonances, which give rise to optical responses that are, at the same time, stronger and more spectrally narrow than those of the localized plasmons of the individual nanostructures. Despite the extensive research effort devoted to investigating the optical properties of lattice resonances, the majority of theoretical studies have analyzed them under plane-wave excitation conditions. Such analysis not only constitutes an approximation to realistic experimental conditions, which require the use of finite-width light beams, but also misses a rich variety of interesting behaviors. Here, we provide a comprehensive study of the response of periodic arrays of metallic nanostructures when excited by finite-width light beams under both paraxial and nonparaxial conditions. We show how as the width of the light beam increases, the response of the array becomes more collective and converges to the plane-wave limit. Furthermore, we analyze the spatial extent of the lattice resonance and identify the optimum values of the light beam width to achieve the strongest optical responses. We also investigate the impact that the combination of finite-size effects in the array and the finite width of the light beam has on the response of the system. Our results provide a solid theoretical framework to understand the excitation of lattice resonances by finite-width light beams and uncover a set of behaviors that do not take place under plane-wave excitation.

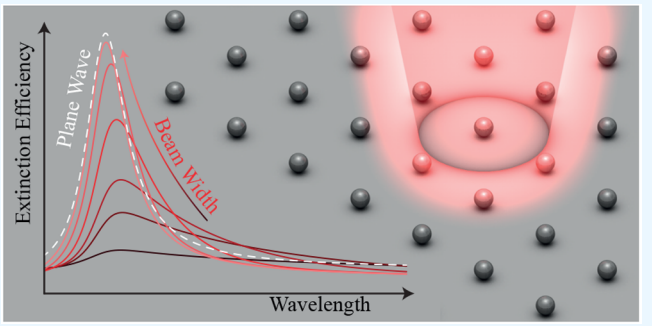

Nanostructures made of metallic materials are well known to support localized plasmons.[1] These excitations interact strongly with light, producing large absorption and scattering cross sections[2] and near-field enhancements,[3] which are being exploited in applications ranging from improved solar energy harvesting[4] and photocatalysis[5] to optical sensing[6] and photothermal cancer therapies.[7] However, the combination of large radiative cross sections and the inherent nonradiative losses of metallic materials usually results in the localized plasmons of individual nanostructures displaying relatively broad lineshapes with quality factors in the range of $Q \lesssim 10-20$.[8−10]

A very promising approach to increase the quality factor and, at the same time, obtain stronger optical responses is to arrange identical metallic nanostructures into a periodic array. By doing so, it is possible to exploit the periodicity of the system to obtain collective modes commonly known as lattice resonances.[9,11−23] These excitations, which arise from the coherent multiple scattering between the localized plasmons supported by the individual nanostructures, appear in the spectrum at wavelengths commensurate with the periodicity of the array[9,20,23,24] and, due to their collective character, produce strong optical responses[25−27] with very narrow lineshapes,[9,20,23,28,29] leading to record quality factors for systems involving metallic materials.[29−38] Thanks to these exceptional properties, the lattice resonances of arrays of metallic nanostructures are the subject of an extensive research effort with a focus on developing novel applications, such as ultrasensitive biosensors,[39−42] different optical elements including lenses,[43] color filters,[44−46] nonlinear[47−50] and light-emitting devices,[51−62] as well as platforms to enhance long-range energy propagation[63−67] or exploring new physical phenomena.[68−71]

However, despite the substantial research effort, the majority of the theoretical studies performed to date have focused on the analysis of the properties of lattice resonances when excited under plane-wave illumination conditions.[9,13,20,21,23] A plane wave is an electromagnetic field with constant amplitude in any plane perpendicular to its propagation direction and, by definition, has an infinite spatial extension.[72] Therefore, a plane wave represents an ideal limit of the electromagnetic field of a collimated light beam and, consequently, constitutes an approximation to any experimental conditions in which the electromagnetic field exciting the array always has a finite extension.[73] It is therefore crucial to understand the conditions under which this approximation is accurate as well as what new behaviors can be obtained when the lattice resonances of

Received: June 20, 2022
Accepted: August 9, 2022

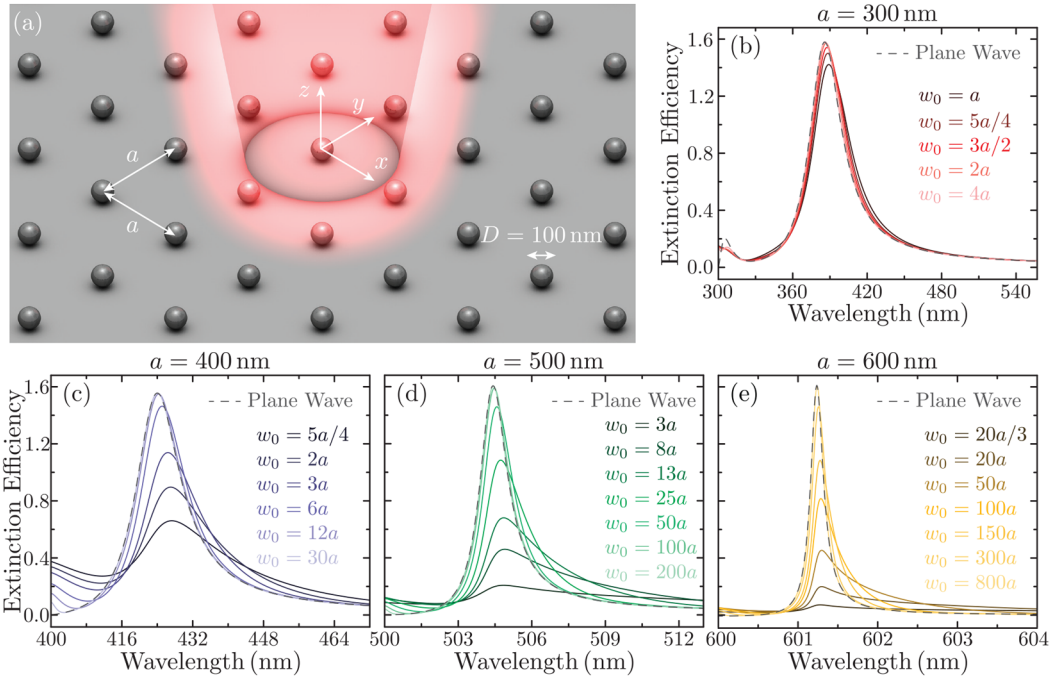

Figure 1. (a) Schematics of the system under consideration, which consists of a periodic array of period a made of silver nanospheres with diameter D = 100 nm. The array is excited by a predominantly x-polarized beam of finite width propagating along the negative z axis and centered at $x = y = 0$. (b−e) Extinction efficiency for arrays with a = 300 (b), 400 (c), 500 (d), and 600 nm (e), calculated for different values of w_0, as indicated by the legends. In all cases, the dashed gray curve shows the response of the array when excited by a plane wave.

periodic arrays of metallic nanostructures are excited by light beams of finite width.

In this article, we provide a detailed theoretical investigation of the optical response of periodic arrays of metallic nanostructures under excitation by finite-width light beams. Specifically, we implement a semianalytical approach based on the combination of the coupled dipole model[13,21,24,29,74−76] and the angular spectrum representation of a light beam,[73] which allows us to describe the excitation of the array by arbitrary light beams under both paraxial and nonparaxial conditions. We show that the optical response associated with the lattice resonance of the array is strongly dependent on the width of the light beam, and, as it increases, the response becomes more collective and approaches the plane-wave limit. Furthermore, we analyze how the width of the light beam affects the spatial extent of the response of the array. Our comprehensive analysis enables us to determine the properties of the light beam that produce the strongest optical responses for both infinite and finite systems. The results of this work provide strong theoretical insight into the excitation of lattice resonances by light beams of finite width, which, in addition to being highly applicable to experimental studies, also reveals a rich variety of behaviors that are not present in the case of plane-wave excitation.

RESULTS AND DISCUSSION

The system under study is depicted in Figure 1a. It consists of a square array of period a made of identical silver nanospheres with diameter D. The array is surrounded by vacuum and located in the xy plane. We assume that the diameter of the nanoparticles D is significantly smaller than both the array period a and the wavelength of light λ, which allows us to describe the response of the array using the coupled dipole model.[13,21,24,29,74−76] Following this approach, we model the nanoparticles as point dipoles with a polarizability α, which we compute from the dipolar Mie scattering coefficient[77] using a tabulated dielectric function.[78] Then, taking into account the interactions between all of the elements of the array, the dipole induced in the nanoparticle located at position $\mathbf{R}_i$ can be written as (see the Methods section)

$$\mathbf{p}_i = \frac{a^2}{4\pi^2}\int_{1\mathrm{BZ}} \mathrm{d}\mathbf{k}_{\parallel}\, \mathcal{A}(\mathbf{k}_{\parallel})\tilde{\mathbf{E}}(\mathbf{k}_{\parallel})e^{i\mathbf{k}_{\parallel}\cdot\mathbf{R}_i} \tag{1}$$

Here, $\mathbf{k}_{\parallel}$ are the components of the wavevector parallel to the array and 1BZ stands for the first Brillouin zone. Furthermore, $\mathcal{A}(\mathbf{k}_{\parallel}) = [\alpha^{-1}\mathcal{I}_{3\times 3} - \mathcal{G}(\mathbf{k}_{\parallel})]^{-1}$ is the polarizability of the array, and $\mathcal{G}(\mathbf{k}_{\parallel})$ is the lattice sum, both defined in the Methods section. The array is excited by a light beam with finite width propagating along the negative z axis and centered at the origin of the xy plane (i.e., $x = y = 0$), whose electric field at $\mathbf{R}_i$ can be expressed using the angular spectrum representation[73] as

$$\mathbf{E}_i = \frac{1}{4\pi^2}\int_{|\mathbf{k}_{\parallel}|\le k} \mathrm{d}\mathbf{k}_{\parallel}\, \mathbf{E}(\mathbf{k}_{\parallel})e^{i\mathbf{k}_{\parallel}\cdot\mathbf{R}_i} \tag{2}$$

To satisfy Maxwell's equations, $\mathbf{E}(\mathbf{k}_{\parallel})$ has to fulfill $\mathbf{E}(\mathbf{k}_{\parallel})\cdot[\mathbf{k}_{\parallel} + k_z\hat{\mathbf{z}}] = 0$ with $k_z = \sqrt{k^2 - |\mathbf{k}_{\parallel}|^2}$ and $k = 2\pi/\lambda$. It is important to remark that this expression is valid under both paraxial and nonparaxial conditions. Throughout this work, we focus on a light beam with a Gaussian intensity profile, for which $\mathbf{E}(\mathbf{k}_{\parallel}) = E_0\,[\hat{\mathbf{x}} - \hat{\mathbf{z}}k_x/k_z]\, f(|\mathbf{k}_{\parallel}|)$ with $f(|\mathbf{k}_{\parallel}|) = 2\pi w_0^2 \exp[-w_0^2|\mathbf{k}_{\parallel}|^2/2]$ and E_0 being a constant. This field is predominantly polarized along the x axis, but the condition $\mathbf{E}(\mathbf{k}_{\parallel})\cdot[\mathbf{k}_{\parallel} + k_z\hat{\mathbf{z}}] = 0$ forces it to have a nonzero longitudinal component. The parameter w_0 controls the width of the light beam, and, as expected, the field defined by eq 2 becomes an x-polarized plane wave in the limit

https://doi.org/10.1021/acsomega.2c03847
ACS Omega XXXX, XXX, XXX−XXX

$w_0 k \gg 1$. Incidentally, $2/(w_0 k)$ could be used to approximately estimate the minimum numerical aperture that would be needed in an experimental setup to create the finite-width light beam with w_0.

Importantly, while the integral in eq 1 spans the first Brillouin zone of the array, the one in eq 2 runs over all $\mathbf{k}_\parallel$ that satisfy $|\mathbf{k}_\parallel| \leq k$ (i.e., it excludes all evanescent waves). Therefore, in order to compute the induced dipole using eq 1, it is necessary to appropriately transform the $\mathbf{k}_\parallel$ components of the electric field amplitude given in eq 2. This can be done by exploiting the periodicity of the array, which allows us to write

$$\tilde{\mathbf{E}}(\mathbf{k}_\parallel) = \frac{1}{a^2} \sum_{\mathbf{q}} \mathbf{E}(\mathbf{k}_\parallel + \mathbf{q}) \tag{3}$$

with the sum running over all of the reciprocal lattice vectors $\mathbf{q} = 2\pi[m\hat{\mathbf{x}} + n\hat{\mathbf{y}}]/a$ (with m and n being integers) that satisfy $|\mathbf{k}_\parallel + \mathbf{q}| \leq k$.

Once we know the dipole induced in the nanoparticles of the array, we can use it to calculate the extinction efficiency of the whole system. This quantity can be written as (see the Methods section)

$$\mathcal{E} = \frac{\omega a^2}{2\pi^2 P_0} \int_{1\mathrm{BZ}} \mathrm{d}\mathbf{k}_\parallel \, \mathrm{Im}\{[\mathcal{A}(\mathbf{k}_\parallel)\tilde{\mathbf{E}}(\mathbf{k}_\parallel)]\cdot\tilde{\mathbf{E}}^*(\mathbf{k}_\parallel)\} \tag{4}$$

where P_0 is the power carried by the light beam exciting the array.

Figure 1b–e displays the extinction efficiency of the lattice resonance with the smallest energy, i.e., the one appearing at the largest wavelength, supported by arrays with $D = 100$ nm and different periods a. There, the colored curves correspond to excitation by a finite-width light beam, while the gray dashed curve shows the plane-wave limit. As indicated by the legends, smaller values of w_0 are represented by darker colored curves, while lighter ones correspond to larger values of w_0. Expectedly, in all cases, the extinction efficiency approaches the plane-wave limit as w_0 is increased. However, the value of w_0 needed to reach the plane-wave limit is strongly dependent on the period of the array a. This can be understood by noting that lattice resonances are associated with the poles of the array polarizability $\mathcal{A}(\mathbf{k}_\parallel)$, which, for excitation with an x-polarized field, appear approximately at wavelengths for which $\mathrm{Re}\{\alpha^{-1} - \mathcal{G}_{xx}(\mathbf{k}_\parallel)\}$ vanishes. While the first term is controlled by the properties of the nanoparticles (scaling as D^{-3} for the nanospheres under consideration), the latter is determined by the geometrical characteristics of the array. In particular, the real part of the lattice sum diverges to $+\infty$ as the wavelength approaches the first Rayleigh anomaly ($\lambda = a$ for $\mathbf{k}_\parallel = 0$) from its red side. Therefore, in order for the array to sustain a collective lattice resonance, $\mathrm{Re}\{\alpha^{-1}\}$ must also take on a positive value of significant magnitude for $\lambda \gtrsim a$. As illustrated in Figure S1 of the Supporting Information, this happens for wavelengths larger than that of the localized plasmon resonance of the individual nanoparticles, and, hence, only the systems for which the localized plasmon occurs on the blue side of the Rayleigh anomaly can support truly collective lattice resonances.[12,74]

This is clearly not the case for the array with $a = 300$ nm since, as shown in Figure S2 of the Supporting Information, the localized plasmon resonance of the individual nanoparticles is located at $\lambda \approx 395$ nm for $D = 100$ nm. As a consequence, its response is mostly dominated by that of the individual nanoparticles, slightly modified by the interaction with their neighbors, and the resonance supported by the array is not collective in nature. The evolution of the extinction spectrum with w_0 confirms this hypothesis: even for the smallest w_0 considered here, $w_0 = a$, the extinction efficiency closely resembles that of the plane-wave limit. It is important to note here that we are able to consider the case of $w_0 = a$ because we use a full nonparaxial description of the light beam rather than relying on the paraxial approximation. On the other hand, the arrays with larger periods, for which the plasmon lies on the blue side of the Rayleigh anomaly, support true lattice resonances and thus require significantly larger values of w_0 to approach the plane-wave limit, with larger values of a requiring wider beams to reach this limit. The reason is that, for a given λ/a, the real part of the lattice sum scales as a^{-3}. Then, as a increases for a fixed value of D, the position of the lattice resonance moves closer to the Rayleigh anomaly, where $\mathrm{Re}\{\mathcal{G}_{xx}(\mathbf{k}_\parallel)\}$ takes larger values. Physically, this means that the lattice resonance becomes more collective,[27] and therefore, it is necessary to simultaneously excite many more nanoparticles to recover the plane-wave limit.

We can gain more insight by explicitly analyzing the properties of the lattice resonances excited by finite-width light beams. Specifically, in Figure 2, we plot the peak value of the extinction efficiency and the quality factor Q for the spectra of Figure 1. The different solid curves display the results corresponding to the different array periods, while the dashed lines show the plane-wave limit. As expected, the extinction efficiency, which is shown in Figure 2a normalized to the

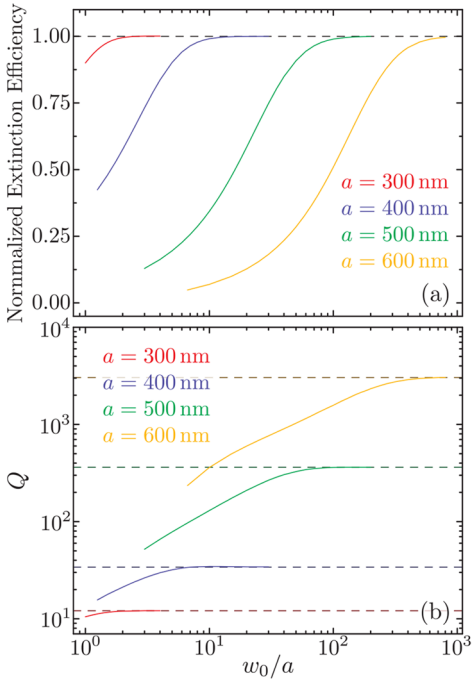

Figure 2. Peak value of the extinction efficiency (a) and quality factor (b) of the lattice resonances supported by the arrays of Figure 1 when excited by a finite-width light beam with different w_0. As indicated by the legend, the different solid curves depict the results for different a, while the dashed lines indicate the corresponding plane-wave limit. The peak value of the extinction efficiency is normalized to the result obtained for the same array under plane-wave excitation.

https://doi.org/10.1021/acsomega.2c03847
ACS Omega XXXX, XXX, XXX−XXX

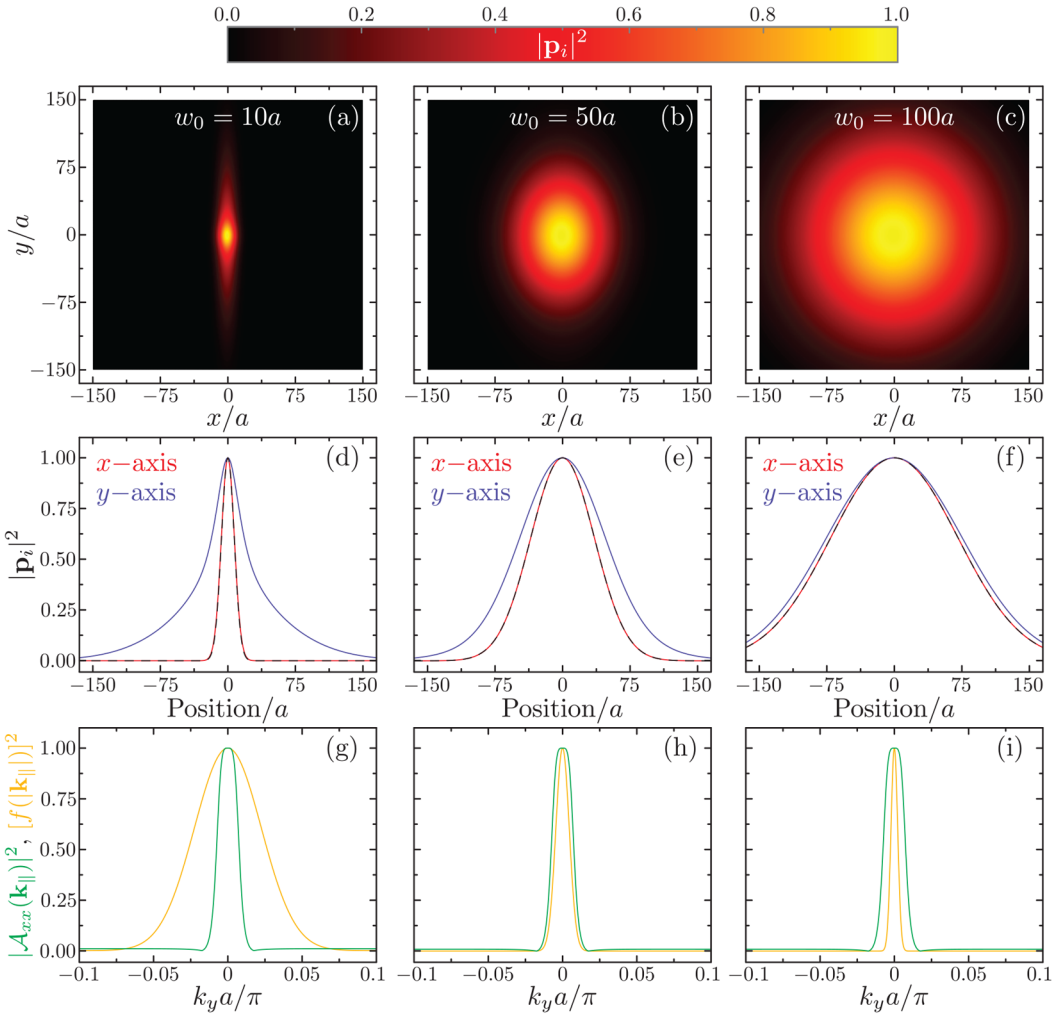

Figure 3. (a−c) Square of the amplitude of the induced dipoles $|\mathbf{p}_i|^2$ for an array with a = 500 nm and D = 100 nm when excited by a finite-width light beam with $w_0 = 10a$ (a), $50a$ (b), and $100a$ (c). In all cases, the induced dipoles are calculated at the wavelength of the lattice resonance and normalized to their largest value. (d−f) Slices of panels a−c along the y axis (blue solid curves) and x axis (red solid curves). The dashed black curves show the value of the normalized electric field intensity of the light beam $|\mathbf{E}_i|^2$. (g−i) Comparison of $|\mathcal{A}_{xx}(\mathbf{k}_\parallel)|^2$ (green curves) and $[f(|\mathbf{k}_\parallel|)]^2$ (yellow curves) as a function of k_y for $k_x = 0$ and for the same w_0 as in a−c. Both quantities are normalized to their maximum value.

plane-wave limit, approaches this limit as w_0 increases. However, as we discussed above, the arrays with larger a require much larger values of w_0 to reach that limit. For example, when the array period is increased from a = 400 nm to a = 600 nm, the value of w_0 needed to approach the plane-wave limit increases by approximately 2 orders of magnitude.

The same general trend is observed in Figure 2b for the quality factor of the resonance, which is defined as the ratio between the wavelength of the resonance and its full-width at half-maximum. Interestingly, before it saturates to the plane-wave limit, the evolution of Q with w_0 appears approximately linear in the figure, which, given the log−log scale, corresponds to a power-law growth. It is also important to note that the values of Q that are achieved in the plane-wave limit vary with a by several orders of magnitude. This is consistent with the scaling $Q \sim (a/D)^9$ of the quality factor of a lattice resonance for $a/D \gg 1$ that we derived in ref 29 for plane-wave excitation. These two behaviors are a direct consequence of the increase in the collective nature of the lattice resonance as the ratio a/D grows.[27] The more collective the lattice resonance gets, the larger its quality factor becomes, but simultaneously, it demands a larger number of nanostructures to be uniformly excited in order to sustain it. This imposes an obvious limitation on the minimum size of the arrays needed for an experiment, since there must be enough nanoparticles for the light beam to excite. Indeed, the interplay between the size of the array and the width of the light beam gives rise to very interesting behaviors that we discuss later.

So far, we have examined the response of the array as a whole, but it is also interesting to consider what occurs at the level of the individual nanoparticles. To that end, in Figure 3a−c, we plot the square of the amplitude of the induced dipoles $|\mathbf{p}_i|^2$ for an array with a = 500 nm and D = 100 nm when excited by light beams with different w_0. In all cases, the induced dipoles are calculated at the wavelength of the lattice resonance and normalized to their maximum value, which, expectedly, is reached in the nanoparticle located at the origin. For $w_0 = 10a$, the spatial distribution of the induced dipoles is highly asymmetric, but for larger values of w_0, the asymmetry becomes less pronounced. This behavior is analyzed in more detail in Figure 3d−f, in which blue and red solid curves display slices of the results of Figure 3a−c along the y and x

https://doi.org/10.1021/acsomega.2c03847
ACS Omega XXXX, XXX, XXX−XXX

axis, respectively. Examining the results for $w_0 = 10a$, we observe that along the y axis the value of $|\mathbf{p}_i|^2$ at a distance of $75a$ remains above 16% of its maximum. However, $|\mathbf{p}_i|^2$ drops below that value at a distance of $\sim 14a$ along the x axis. This difference gradually decreases as w_0 takes larger values. At the same time, the spatial distribution of the induced dipoles extends farther away from the origin and its shape becomes closer to a Gaussian profile. For comparison, the black dashed curves display the normalized electric field intensity of the light beam $|\mathbf{E}_i|^2$, which, for the values of w_0 under consideration, takes indistinguishable values along the y and x axes. Importantly, in all cases, the spatial extension of the distribution of $|\mathbf{p}_i|^2$ along the y axis clearly exceeds that of $|\mathbf{E}_i|^2$, although it does so by a smaller degree for larger w_0. On the contrary, they perfectly match along the x axis.

In order to understand all of these behaviors, we need to consider that lattice resonances originate from the far-field coupling between the elements of the array, which is maximum along the axis perpendicular to the dipole moment induced in the nanoparticles.[67] As discussed above, the electric field of the light beam that we consider in this work is mainly polarized along the x axis (see eq 2), and therefore, the lattice resonance excited in the array propagates predominantly along the y axis. This explains the strongly asymmetric spatial distribution of $|\mathbf{p}_i|^2$ observed for the smallest value of w_0. The asymmetry is reduced as w_0 increases, and consequently, the width of the light beam becomes first comparable to and then larger than the propagation length of the lattice resonance. When that happens, the shape of the spatial distribution of the induced dipole closely follows the profile of the electric field intensity of the light beam.

To further support this explanation, we examine the response of both the array and the light beam in reciprocal space. In particular, Figure 3g–i shows the values of $|\mathcal{A}_{xx}(\mathbf{k}_\parallel)|^2$ (green curves), which characterizes the intrinsic response of the array, and $[f(|\mathbf{k}_\parallel|)]^2$ (yellow curves), which defines the profile of the electric field intensity of the light beam, both as a function of k_y for $k_x = 0$ and normalized to their maximum value. Notice that the inverse of the width of $|\mathcal{A}_{xx}(\mathbf{k}_\parallel)|^2$ can be associated with an effective propagation length for the lattice resonance. Comparing the two quantities, we observe that, while for $w_0 = 10a$, $[f(|\mathbf{k}_\parallel|)]^2$ is much broader than the array polarizability, the opposite is true for $w_0 = 100a$. This confirms that, as w_0 increases, the spatial distribution of the induced dipoles transitions from being determined by the lattice resonance of the array to being determined by the characteristics of the light beam. Importantly, the fact that, for certain values of w_0, the induced dipoles take significant values even beyond the spatial extent of the light beam can be used experimentally to excite areas of the array that are not directly illuminated by it.

Our analysis of the results displayed in Figure 3 has revealed that the spatial distribution of the induced dipoles has a nontrivial dependence with w_0 and that, in particular, many interesting behaviors emerge at the level of the individual nanoparticles as w_0 varies. Motivated by this, in Figure 4, we investigate the optimal value of w_0 that produces the maximum optical response in a cluster of nanoparticles constituting a subset of the full array. To do so, we define the following function

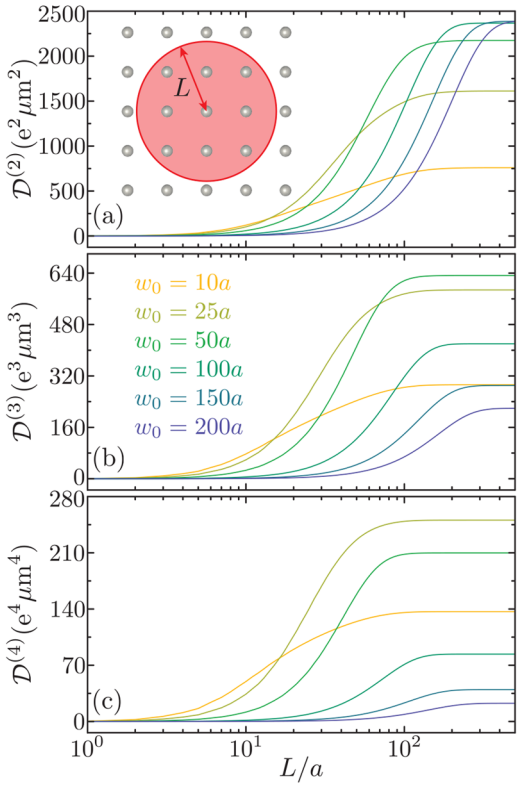

Figure 4. (a–c) Value of $\mathcal{D}^{(n)}$, defined in eq 5, as a function of L for $n = 2$ (a), 3 (b), and 4 (c). All calculations are performed for an array with $a = 500$ nm and $D = 100$ nm and different values of w_0, as indicated by the legend.

$$\mathcal{D}^{(n)} = \sum_i |\mathbf{p}_i|^n \tag{5}$$

where the sum runs over all of the nanoparticles located at a distance from the origin smaller than L, i.e., those satisfying $|\mathbf{R}_i| \leq L$, as indicated in the inset of Figure 4a. For $n = 2$, this function characterizes the linear response of the cluster. In particular, $\mathcal{D}^{(2)}$ is proportional to the total power absorbed by the nanoparticles in the cluster. On the other hand, for $n > 2$, this function provides different estimates of the nonlinear response of the cluster. It is important to note that in order to obtain a meaningful comparison between light beams with different w_0, we choose E_0 such that all of them carry the same total power. Figure 4a shows the results for $n = 2$ in units of $e^2\,\mu m^2$, with e being the elementary charge. We consider an array with $a = 500$ nm and $D = 100$ nm and, as indicated by the legend, the different colored curves show the results obtained for different values of w_0. Examining these results, we observe that, when $L < 10a$, the largest values of $\mathcal{D}^{(2)}$ are obtained for the beam with the smallest w_0. However, as the size of the cluster grows, the optimum value of w_0 continuously increases. Indeed, we can infer from the results that, for a given L, the largest values of $\mathcal{D}^{(2)}$ are obtained for light beams with $w_0 \gtrsim L$. Expectedly, this trend saturates as the response of the system reaches the plane-wave limit, which, for the array under consideration, occurs for $w_0 \approx 150a$. We can explain all of these results by considering two competing mechanisms: on one hand, smaller values of w_0 result in a higher intensity directed at the nanoparticles of the cluster and, hence, a larger

https://doi.org/10.1021/acsomega.2c03847
ACS Omega XXXX, XXX, XXX−XXX

individual response, but, on the other hand, as w_0 grows, the response of the array becomes more collective and therefore the strength of the lattice resonance increases, as demonstrated in Figures 1 and 2. Consequently, as L grows, the second mechanism increasingly dominates the response of the cluster, thus favoring larger values of w_0.

The behavior of $\mathcal{D}^{(n)}$ for $n > 2$ is analyzed in Figure 4b and 4c, which shows, respectively, the values of $\mathcal{D}^{(3)}$ and $\mathcal{D}^{(4)}$. For a small cluster size, the behavior is similar to that of the $n = 2$ case. However, as L grows, we observe that $\mathcal{D}^{(3)}$ and $\mathcal{D}^{(4)}$ reach their largest values for $w_0 = 50a$ and $25a$, respectively, and then continuously decrease as w_0 further grows. This is a direct consequence of the larger exponent in the induced dipole, which favors having a larger intensity on the nanoparticles of the cluster over the collective enhancement provided by the lattice resonances. Therefore, we conclude that, as the size of the cluster increases, its linear response is enhanced by the collective nature of the lattice resonance and therefore grows with w_0. On the contrary, for a response associated with a larger value of n, there appears to be optimum values of w_0 that maximize it. These results have important implications for experimental techniques such as surface-enhanced Raman scattering (SERS) spectroscopy, since they suggest that, under certain conditions, the optimal excitation scenario is not necessarily a plane wave, but rather a light beam of finite width.

One important aspect that we need to consider is that, although arrays of nanoparticles are usually modeled as perfectly periodic and, hence, infinite systems, they must have a finite size in any experimental realization. This can lead to significant discrepancies between their optical response and the theoretical predictions obtained for infinite arrays. Such discrepancies, commonly known as finite-size effects, arise from the presence of edges as well as from the truncation of the collective behavior due to the finiteness of the structure. Several works have investigated the impact of finite-size effects on the response of periodic arrays of metallic nanoparticles under plane-wave excitation conditions.[29,76,79−81] Then, it is very interesting to extend these studies to the cases in which the array is excited by a light beam with finite width and, in particular, investigate the effects arising from the interplay between the size of the array and the extension of the beam.

To that end, in Figure 5, we plot the peak value of the extinction efficiency and the quality factor Q of the lattice resonance supported by a finite array with $N \times N$ nanoparticles when excited by a light beam with different w_0. These results are extracted from the extinction spectra plotted in Figure S3 of the Supporting Information (see the Methods section for details of the calculation). In all cases, the array has $a = 400$ nm and $D = 100$ nm and, as indicated by the legend, the different colored curves correspond to different values of N. Examining the peak extinction efficiency shown in Figure 5a, which is normalized to the value obtained for the same array under plane-wave excitation, we observe two very interesting behaviors. First, the extinction efficiency reaches a maximum at a certain value of w_0 and then becomes smaller as w_0 is further increased. Second, in some cases, the maximum value of the normalized extinction efficiency reaches values above one. This means that, when excited by the appropriate finite-width light beam, the extinction efficiency of the lattice resonance supported by finite arrays can surpass that obtained under plane-wave excitation conditions. Both of these

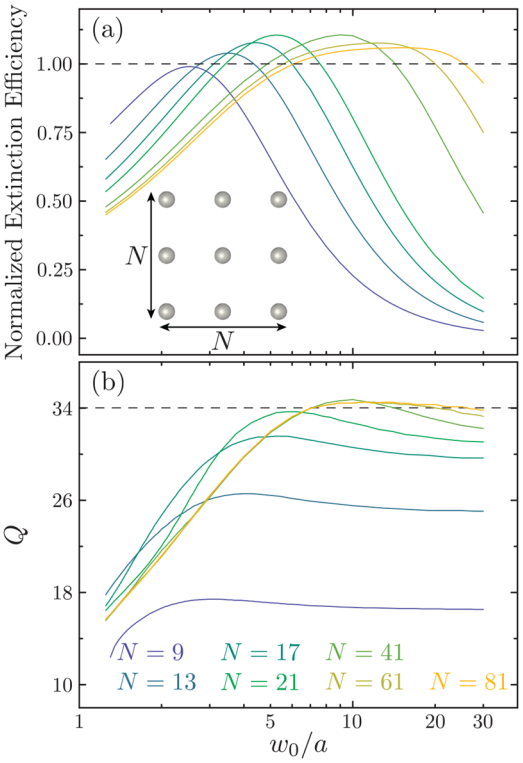

Figure 5. Peak value of the extinction efficiency (a) and quality factor (b) of the lattice resonance of a finite array with $N \times N$ nanoparticles when excited by a finite-width light beam with different w_0. In all cases, the array under consideration has $a = 400$ nm and $D = 100$ nm. As indicated by the legend, the different colored curves depict the results for different values of N. The peak value of the extinction efficiency is normalized to the result obtained for the same array under plane-wave excitation.

behaviors are in sharp contrast with the results obtained for infinite arrays, for which, as shown in Figure 2, the maximum extinction efficiency is always reached at the plane-wave limit.

The quality factor of the lattice resonance, which is analyzed in Figure 5b, also displays a maximum, although, as opposed to the extinction efficiency, its value does not significantly decrease for larger values of w_0. Expectedly, Q increases as N grows, approaching the value for the infinite array under plane-wave excitation, which is indicated by the black dashed line. Indeed, we know from previous works that, for plane-wave excitation, both the extinction efficiency and the quality factor become larger with the size of the array due to the increase of the collective nature of the lattice resonance that they support.[29,76] As shown by both Figure S3 of the Supporting Information and Figure 5b, that behavior is clearly preserved under excitation by a finite-width light beam. However, in this case, for a given N, there exists an optimum value of w_0 such that the spatial extension of the light beam is large enough to maximize the collective behavior of the lattice resonance but, at the same time, it concentrates as much intensity as possible in the area covered by the finite array. Therefore, this interplay between the size of the array and the width of the light beam is what gives rise to the interesting results shown in Figure 5. Furthermore, these results highlight the importance, for any experimental realization of these systems, of using a light beam with a width that is appropriately tailored to the finite size of the array.

https://doi.org/10.1021/acsomega.2c03847
ACS Omega XXXX, XXX, XXX−XXX

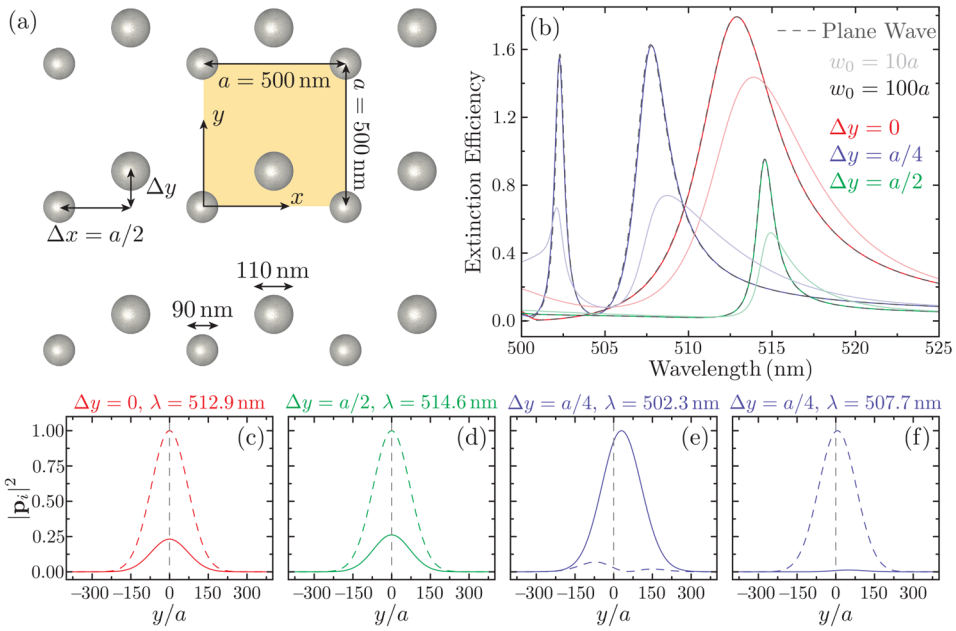

Figure 6. (a) Schematics of the bipartite array under consideration, which is built from the periodic repetition of a unit cell containing two silver nanospheres (shaded area) over a square lattice of period a = 500 nm. The smaller nanoparticle has a diameter of 90 nm and is located at the origin of the unit cell, while the larger one has a diameter of 110 nm and is placed at a distance $\mathbf{d} = \Delta x\hat{\mathbf{x}} + \Delta y\hat{\mathbf{y}}$ from the other nanoparticle. (b) Extinction efficiency for the bipartite array when excited by either a plane wave (gray dashed curves) or a finite-width light beam with $w_0 = 10a$ (light solid curves) or $w_0 = 100a$ (dark solid curves). As indicated by the legend, the red, blue, and green curves correspond to bipartite arrays with $\Delta y = 0$, $a/4$, and $a/2$, respectively, while $\Delta x = a/2$ in all cases. (c−f) Spatial dependence of the square of the amplitude of the induced dipoles $|\mathbf{p}_i|^2$ along the y axis for the bipartite array with $\Delta y = 0$ (c), $a/2$ (d), and $a/4$ (e, f). All induced dipoles are calculated at the wavelengths of the lattice resonances indicated above the panel, assuming that $w_0 = 100a$, and are normalized to the largest value. The solid and dashed curves represent the values corresponding to the smaller and larger nanoparticles, respectively.

All of the arrays we have investigated so far are made of the repetition of a unit cell with a single nanoparticle. However, arrays with multiparticle unit cells have been shown to display very interesting optical responses.[19,22,24,37,82−86] These systems can support lattice resonances with properties that are fully controlled by the size and relative position of the nanoparticles in the unit cell.[24] It is therefore very relevant to investigate how these lattice resonances behave when excited by a light beam with a finite width. To fulfill this goal, we analyze the response of the bipartite array depicted in Figure 6a. This array is made from the repetition over a square lattice of period a = 500 nm of a unit cell (shaded area) composed of two silver nanospheres with diameters of 90 and 110 nm. The smaller nanoparticle is located at the origin of the unit cell, while the larger one is placed at a distance $\mathbf{d} = \Delta x\hat{\mathbf{x}} + \Delta y\hat{\mathbf{y}}$ with $\Delta x = a/2$.

The bipartite array supports lattice resonances with very different properties depending on the value of Δy, as shown in Figure 6b. There, we plot the extinction efficiency for $\Delta y = 0$, $a/4$, and $a/2$ using the different colors indicated by the legend. In all cases, the light and dark solid colored curves represent the results obtained for excitation by a finite-width light beam with $w_0 = 10a$ and $100a$, respectively, while the dashed gray curves indicate the results under plane-wave excitation. To perform these calculations, we extended eqs 1, 2, and 4 to account for multiparticle unit cells, following the approach described in refs 24 and 29. Examining the extinction efficiency spectra, we observe that, for both $\Delta y = 0$ and $\Delta y = a/2$, the system supports a single lattice resonance. However, while the resonance of the former is characterized by a broad linewidth and a large peak extinction efficiency, the latter displays the exact opposite characteristics. These resonances correspond, respectively, to the super- and subradiant lattice resonances described in ref 29, in which the dipoles induced in the nanoparticles oscillate in phase and in antiphase. On the other hand, for $\Delta y = a/4$, the system supports two different lattice resonances, each of which corresponds to the lattice resonance of one of the two single-particle arrays into which the bipartite array can be separated.[24,29]

Importantly, for all of the cases under investigation, the extinction efficiency spectrum for $w_0 = 100a$ completely matches that obtained for plane-wave excitation. However, for $w_0 = 10a$, the extinction efficiency reaches smaller peak values and the quality factor deteriorates significantly. These results reveal the collective nature of the lattice resonances supported by bipartite arrays and confirm that their optical response evolves in the same way as that of their single-particle counterparts when excited by light beams of finite width.

To complete our analysis, in Figure 6c−f, we examine the response of the lattice resonances of the bipartite array at the level of the individual nanoparticles. We do so by analyzing the square of the amplitude of the dipole induced in the nanoparticles of the unit cells located along the y axis for the different arrays considered in Figure 6a. In all cases, the arrays are excited by a finite-width light beam with $w_0 = 100a$ and the calculations are performed at the wavelength of the lattice resonance, which is indicated above each of the panels. We use solid and dashed curves to display the value of $|\mathbf{p}_i|^2$ for the smaller and larger nanoparticles, respectively. As discussed above, the lattice resonances supported by the arrays with Δy = 0 and $a/2$ involve the simultaneous excitation of the two nanoparticles in the unit cell, with the only difference being

https://doi.org/10.1021/acsomega.2c03847
ACS Omega XXXX, XXX, XXX−XXX

their relative phase. Consequently, the spatial distributions of the induced dipole, shown, respectively, in Figure 6c and 6d, are visually identical, with the larger particle displaying a larger value of $|\mathbf{p}_i|^2$ due to its larger polarizability. As expected, these distributions follow the Gaussian profile of the finite-width light beam and are peaked at the origin, where the field reaches its maximum value.

The behavior is different for the array with $\Delta y = a/4$. This system supports two lattice resonances, which produce the spatial distributions of $|\mathbf{p}_i|^2$ shown in Figure 6e and 6f. As expected, the first lattice resonance, which occurs closer to the Rayleigh anomaly, is sustained by the smaller nanoparticles, while for the second one, the situation is completely reversed. Examining these results more closely, we can see that, in both cases, the spatial distribution of $|\mathbf{p}_i|^2$ for the nanoparticle sustaining the lattice resonance follows a Gaussian shape, while the distribution for the other nanoparticle in the unit cell displays a more complicated one. Interestingly, the largest induced dipole does not occur in the nanoparticles located at the origin, even though that is where the field of the light beam is maximum. On the contrary, the maximum induced dipole is reached at a unit cell located in the positive part of the y axis. This behavior can be attributed to the fact that, as opposed to the other two systems, the array with $\Delta y = a/4$ is not symmetric under inversion over the x axis. While this characteristic is irrelevant for plane-wave excitation, it does induce a spatially asymmetric response when the array is excited by a finite-width light beam. These results highlight, once again, the nontrivial behavior of lattice resonances when excited by finite-width light beams.

CONCLUSIONS

In summary, we have performed a comprehensive analysis of the behavior of the lattice resonances supported by periodic arrays of nanoparticles when excited by light beams of finite width. To do so, we have implemented a theoretical approach based on the combination of the coupled dipole model and the angular spectrum representation, which, despite its simplicity, provides a rigorous description of the excitation of periodic arrays by arbitrary light beams under paraxial as well as nonparaxial conditions. Using this approach, we have shown that the optical response produced by the lattice resonances of the array is strongly dependent on the width of the light beam that excites them. As the width of the light beam increases and hence approaches the plane-wave limit, the response becomes more collective, giving rise to larger extinction efficiencies and quality factors. Interestingly, the width at which the plane-wave limit is reached can vary by orders of magnitude depending on the characteristics of the array. Furthermore, we have found that when the propagation length of the lattice resonance exceeds the width of the light beam, the spatial response of the array displays a significant asymmetry, extending farther away in the direction perpendicular to the polarization of the light beam. We have also identified the optimum characteristics of a light beam to produce the strongest optical responses in both finite and infinite systems, revealing a complicated interplay between the size of the array and the extension of the beam that excites it. Finally, we have extended our analysis to the lattice resonances of bipartite arrays, for which, depending on the geometry of their unit cell, excitation by finite-width light beams can result in symmetry breaking effects. Although we have focused on arrays of metallic nanoparticles, our theoretical approach can be readily extended to arrays made of other elements, such as dielectric nanostructures[87] or atoms,[88−90] by using the appropriate polarizability. This work establishes a solid theoretical framework to understand the excitation of lattice resonances by light beams of finite-width, revealing a range of behaviors that are not present under plane-wave excitation. Due to the realistic nature of the finite-width light beams we consider, our results are highly relevant to any experimental efforts dedicated to exploiting the extraordinary optical properties of lattice resonances.

METHODS

Derivation of the Induced Dipole. Within the dipolar approximation, we describe the response of each of the nanospheres using a point dipole with polarizability α. Then, following the coupled dipole model,[13,21,24,29,74−76] we can write the dipole induced in the nanoparticle located at position $\mathbf{R}_i$ as

$$\mathbf{p}_i = \alpha \mathbf{E}_i + \alpha \sum_{j \neq i} \mathbf{G}_{ij} \mathbf{p}_j \tag{6}$$

Here, $\mathbf{E}_i$ is the external field at the nanoparticle, $\mathbf{G}_{ij} = [k^2 \mathcal{I}_{3\times 3} + \nabla\nabla] e^{ik|\mathbf{R}_i - \mathbf{R}_j|}/|\mathbf{R}_i - \mathbf{R}_j|$ is the Green tensor of vacuum, and $k = 2\pi/\lambda$ (notice that we use Gaussian units). For an infinite array of period a, we can exploit its periodicity and use the Fourier transform defined as $v_i = \frac{a^2}{4\pi^2} \int_{1\mathrm{BZ}} d\mathbf{k}_{\parallel} v(\mathbf{k}_{\parallel}) e^{i\mathbf{k}_{\parallel}\cdot\mathbf{R}_i}$, where the integral runs over the first Brillouin zone. By doing so, we transform eq 6 into the following self-consistent expression for the $\mathbf{k}_{\parallel}$ components of the dipole induced in the nanoparticles

$$\mathbf{p}(\mathbf{k}_{\parallel}) = \alpha \tilde{\mathbf{E}}(\mathbf{k}_{\parallel}) + \alpha \mathcal{G}(\mathbf{k}_{\parallel}) \mathbf{p}(\mathbf{k}_{\parallel}) \tag{7}$$

where $\mathcal{G}(\mathbf{k}_{\parallel}) = \sum_{j\neq i} \mathbf{G}_{ij} e^{-i\mathbf{k}_{\parallel}\cdot(\mathbf{R}_i - \mathbf{R}_j)}$ is known as the lattice sum. Then, solving eq 7, we obtain $\mathbf{p}(\mathbf{k}_{\parallel}) = \mathcal{A}(\mathbf{k}_{\parallel}) \tilde{\mathbf{E}}(\mathbf{k}_{\parallel})$, with $\mathcal{A}(\mathbf{k}_{\parallel}) = [\alpha^{-1} \mathcal{I}_{3\times 3} - \mathcal{G}(\mathbf{k}_{\parallel})]^{-1}$ being the polarizability of the array. In the case of a finite array, eq 6 can be directly solved to obtain $\mathbf{p}_i = \sum_j \mathbf{A}_{ij} \mathbf{E}_j$ with $\mathbf{A}_{ij} = [\alpha^{-1} \mathcal{I}_{3N\times 3N} - \mathbf{G}]^{-1}_{ij}$.

Derivation of the Extinction Efficiency of the Array. We can calculate $\mathcal{E}$ by summing the extinction efficiency of each of the dipoles in the array: $\mathcal{E} = \sum_i 2\omega \mathrm{Im}\{\mathbf{p}_i \cdot \mathbf{E}_i^*\}/P_0$. For an infinite array, we can substitute the expressions of the dipole and field given in eqs 1 and 2, respectively, and use $\sum_i e^{i(\mathbf{k}_{\parallel} - \mathbf{k}_{\parallel}')\cdot\mathbf{R}_i} = \frac{4\pi^2}{a^2} \sum_{\mathbf{q}} \delta(\mathbf{k}_{\parallel} - \mathbf{k}_{\parallel}' + \mathbf{q})$ to obtain the result of eq 4.

ASSOCIATED CONTENT

Supporting Information

The Supporting Information is available free of charge at https://pubs.acs.org/doi/10.1021/acsomega.2c03847.

Analysis of the origin of the lattice resonance within the coupled dipole model; extinction cross section of an individual nanoparticle; extinction efficiency spectra for finite arrays of nanoparticles excited by either finite-width light beams with different w_0 or a plane wave (PDF)

https://doi.org/10.1021/acsomega.2c03847
ACS Omega XXXX, XXX, XXX−XXX

AUTHOR INFORMATION

Corresponding Author

Alejandro Manjavacas − *Instituto de Óptica (IO-CSIC), Consejo Superior de Investigaciones Científicas, 28006 Madrid, Spain; Department of Physics and Astronomy, University of New Mexico, Albuquerque, New Mexico 87106, United States;* orcid.org/0000-0002-2379-1242; Email: a.manjavacas@csic.es

Authors

Lauren Zundel − *Department of Physics and Astronomy, University of New Mexico, Albuquerque, New Mexico 87106, United States;* orcid.org/0000-0003-1850-5210

Juan R. Deop-Ruano − *Instituto de Óptica (IO-CSIC), Consejo Superior de Investigaciones Científicas, 28006 Madrid, Spain;* orcid.org/0000-0002-2613-5873

Rosario Martinez-Herrero − *Departamento de Óptica, Universidad Complutense de Madrid, 28040 Madrid, Spain*

Complete contact information is available at: https://pubs.acs.org/10.1021/acsomega.2c03847

Author Contributions

§L.Z. and J.R.D.-R.: These authors contributed equally to this paper.

Notes

The authors declare no competing financial interest.

ACKNOWLEDGMENTS

This work was sponsored by a Leonardo Grant for Researchers in Physics from the BBVA Foundation. The authors also acknowledge support from Grant Nos. PID2019-104268GB-C21 and PID2019-109502GA-I00 funded by MCIN/AEI/10.13039/501100011033 as well as the U.S. National Science Foundation (Grant No. DMR-1941680). L.Z. acknowledges support from the Department of Energy Computational Science Graduate Fellowship (Grant No. DE-SC0020347). J.R.D.-R. acknowledges a predoctoral fellowship from the MCIN/AEI assigned to Grant No. PID2019-109502GA-I00. We also thank the UNM Center for Advanced Research Computing, supported in part by the U.S. National Science Foundation, for providing some of the computational resources used in this work.

REFERENCES

(1) Maier, S. A. *Plasmonics: Fundamentals and Applications*; Springer: New York, 2007.

(2) Myroshnychenko, V.; Rodríguez-Fernández, J.; Pastoriza-Santos, I.; Funston, A. M.; Novo, C.; Mulvaney, P.; Liz-Marzán, L. M.; García de Abajo, F. J. Modelling the optical response of gold nanoparticles. *Chem. Soc. Rev.* **2008**, *37*, 1792−1805.

(3) Álvarez-Puebla, R. A.; Liz-Marzán, L. M.; García de Abajo, F. J. Light concentration at the nanometer scale. *J. Phys. Chem. Lett.* **2010**, *1*, 2428−2434.

(4) Atwater, H. A.; Polman, A. Plasmonics for improved photovoltaic devices. *Nat. Mater.* **2010**, *9*, 205−213.

(5) Brongersma, M. L.; Halas, N. J.; Nordlander, P. Plasmon-induced hot carrier science and technology. *Nat. Nanotechnol.* **2015**, *10*, 25−34.

(6) Ding, S.-Y.; You, E.-M.; Tian, Z.-Q.; Moskovits, M. Electromagnetic theories of surface-enhanced Raman spectroscopy. *Chem. Soc. Rev.* **2017**, *46*, 4042−4076.

(7) Rastinehad, A. R.; et al. Gold nanoshell-localized photothermal ablation of prostate tumors in a clinical pilot device study. *Proc. Natl. Acad. Sci. U. S. A.* **2019**, *116*, 18590−18596.

(8) Derom, S.; Vincent, R.; Bouhelier, A.; Colas des Francs, G. Resonance quality, radiative/ohmic losses and modal volume of Mie plasmons. *Europhys. Lett.* **2012**, *98*, 47008.

(9) Kravets, V. G.; Kabashin, A. V.; Barnes, W. L.; Grigorenko, A. N. Plasmonic surface lattice resonances: a review of properties and applications. *Chem. Rev.* **2018**, *118*, 5912−5951.

(10) Doiron, B.; Mota, M.; Wells, M. P.; Bower, R.; Mihai, A.; Li, Y.; Cohen, L. F.; Alford, N. M.; Petrov, P. K.; Oulton, R. F.; Maier, S. A. Quantifying figures of merit for localized surface plasmon resonance applications: a materials survey. *ACS Photonics* **2019**, *6*, 240−259.

(11) Zhao, L.; Kelly, K. L.; Schatz, G. C. The extinction spectra of silver nanoparticle arrays: influence of array structure on plasmon resonance wavelength and width. *J. Phys. Chem. B* **2003**, *107*, 7343−7350.

(12) Zou, S.; Janel, N.; Schatz, G. C. Silver nanoparticle array structures that produce remarkably narrow plasmon lineshapes. *J. Chem. Phys.* **2004**, *120*, 10871−10875.

(13) García de Abajo, F. J. Colloquium: Light scattering by particle and hole arrays. *Rev. Mod. Phys.* **2007**, *79*, 1267−1290.

(14) Auguié, B.; Barnes, W. L. Collective resonances in gold nanoparticle arrays. *Phys. Rev. Lett.* **2008**, *101*, 143902.

(15) Kravets, V. G.; Schedin, F.; Grigorenko, A. N. Extremely narrow plasmon resonances based on diffraction coupling of localized plasmons in arrays of metallic nanoparticles. *Phys. Rev. Lett.* **2008**, *101*, 087403.

(16) Chu, Y.; Schonbrun, E.; Yang, T.; Crozier, K. B. Experimental observation of narrow surface plasmon resonances in gold nanoparticle arrays. *Appl. Phys. Lett.* **2008**, *93*, 181108.

(17) Vecchi, G.; Giannini, V.; Gómez Rivas, J. Surface modes in plasmonic crystals induced by diffractive coupling of nanoantennas. *Phys. Rev. B* **2009**, *80*, 201401R.

(18) Humphrey, A. D.; Meinzer, N.; Starkey, T. A.; Barnes, W. L. Surface lattice resonances in plasmonic arrays of asymmetric disc dimers. *ACS Photonics* **2016**, *3*, 634−639.

(19) Humphrey, A. D.; Barnes, W. L. Plasmonic surface lattice resonances in arrays of metallic nanoparticle dimers. *J. Opt.* **2016**, *18*, 035005.

(20) Wang, W.; Ramezani, M.; Väkeväinen, A. I.; Törmä, P.; Gómez Rivas, J.; Odom, T. W. The rich photonic world of plasmonic nanoparticle arrays. *Mater. Today* **2018**, *21*, 303−314.

(21) Cherqui, C.; Bourgeois, M. R.; Wang, D.; Schatz, G. C. Plasmonic surface lattice resonances: theory and computation. *Acc. Chem. Res.* **2019**, *52*, 2548−2558.

(22) Fradkin, I. M.; Dyakov, S. A.; Gippius, N. A. Nanoparticle lattices with bases: Fourier modal method and dipole approximation. *Phys. Rev. B* **2020**, *102*, 045432.

(23) Utyushev, A. D.; Zakomirnyi, V. I.; Rasskazov, I. L. Collective lattice resonances: Plasmonics and beyond. *Rev. Phys.* **2021**, *6*, 100051.

(24) Baur, S.; Sanders, S.; Manjavacas, A. Hybridization of lattice resonances. *ACS Nano* **2018**, *12*, 1618−1629.

(25) Zou, S.; Schatz, G. C. Silver nanoparticle array structures that produce giant enhancements in electromagnetic fields. *Chem. Phys. Lett.* **2005**, *403*, 62−67.

(26) Nikitin, A. G.; Kabashin, A. V.; Dallaporta, H. Plasmonic resonances in diffractive arrays of gold nanoantennas: near and far field effects. *Opt. Express* **2012**, *20*, 27941−27952.

(27) Manjavacas, A.; Zundel, L.; Sanders, S. Analysis of the limits of the near-field produced by nanoparticle arrays. *ACS Nano* **2019**, *13*, 10682−10693.

(28) Scarabelli, L.; Vila-Liarte, D.; Mihi, A.; Liz-Marzán, L. M. Templated colloidal self-assembly for lattice plasmon engineering. *Acc. Mater. Res.* **2021**, *2*, 816−827.

(29) Cuartero-González, A.; Sanders, S.; Zundel, L.; Fernández-Domínguez, A. I.; Manjavacas, A. Super- and subradiant lattice resonances in bipartite nanoparticle arrays. *ACS Nano* **2020**, *14*, 11876.

(30) Adato, R.; Yanik, A. A.; Wu, C.-H.; Shvets, G.; Altug, H. Radiative engineering of plasmon lifetimes in embedded nanoantenna arrays. *Opt. Express* **2010**, *18*, 4526−4537.
(31) Zakomirnyi, V. I.; Rasskazov, I. L.; Gerasimov, V. S.; Ershov, A. E.; Polyutov, S. P.; Karpov, S. V. Refractory titanium nitride two-dimensional structures with extremely narrow surface lattice resonances at telecommunication wavelengths. *Appl. Phys. Lett.* **2017**, *111*, 123107.
(32) Khlopin, D.; Laux, F.; Wardley, W. P.; Martin, J.; Wurtz, G. A.; Plain, J.; Bonod, N.; Zayats, A. V.; Dickson, W.; Gérard, D. Lattice modes and plasmonic linewidth engineering in gold and aluminum nanoparticle arrays. *J. Opt. Soc. Am. B* **2017**, *34*, 691−700.
(33) Le-Van, Q.; Zoethout, E.; Geluk, E.-J.; Ramezani, M.; Berghuis, M.; Gómez Rivas, J. Enhanced quality factors of surface lattice resonances in plasmonic arrays of nanoparticles. *Adv. Opt. Mater.* **2019**, *7*, 1801451.
(34) Zhu, X.; Imran Hossain, G. M.; George, M.; Farhang, A.; Cicek, A.; Yanik, A. A. Beyond noble metals: high q-factor aluminum nanoplasmonics. *ACS Photonics* **2020**, *7*, 416−424.
(35) Deng, S.; Li, R.; Park, J.-E.; Guan, J.; Choo, P.; Hu, J.; Smeets, P. J. M.; Odom, T. W. Ultranarrow plasmon resonances from annealed nanoparticle lattices. *Proc. Natl. Acad. Sci. U. S. A.* **2020**, *117*, 23380−23384.
(36) Bin-Alam, M. S.; Reshef, O.; Mamchur, Y.; Alam, M. Z.; Carlow, G.; Upham, J.; Sullivan, B. T.; Ménard, J.-M.; Huttunen, M. J.; Boyd, R. W.; Dolgaleva, K. Ultra-high-Q resonances in plasmonic metasurfaces. *Nat. Commun.* **2021**, *12*, 974.
(37) Zundel, L.; May, A.; Manjavacas, A. Lattice resonances induced by periodic vacancies in arrays of nanoparticles. *ACS Photonics* **2021**, *8*, 360−368.
(38) Molet, P.; Passarelli, N.; Pérez, L. A.; Scarabelli, L.; Mihi, A. Engineering plasmonic colloidal meta-molecules for tunable photonic supercrystals. *Adv. Opt. Mater.* **2021**, *9*, 2100761.
(39) Adato, R.; Yanik, A. A.; Amsden, J. J.; Kaplan, D. L.; Omenetto, F. G.; Hong, M. K.; Erramilli, S.; Altug, H. Ultra-sensitive vibrational spectroscopy of protein monolayers with plasmonic nanoantenna arrays. *Proc. Natl. Acad. Sci. U. S. A.* **2009**, *106*, 19227−19232.
(40) Thackray, B. D.; Kravets, V. G.; Schedin, F.; Auton, G.; Thomas, P. A.; Grigorenko, A. N. Narrow collective plasmon resonances in nanostructure arrays observed at normal light incidence for simplified sensing in asymmetric air and water environments. *ACS Photonics* **2014**, *1*, 1116−1126.
(41) Danilov, A.; Tselikov, G.; Wu, F.; Kravets, V. G.; Ozerov, I.; Bedu, F.; Grigorenko, A. N.; Kabashin, A. V. Ultra-narrow surface lattice resonances in plasmonic metamaterial arrays for biosensing applications. *Biosens. Bioelectron.* **2018**, *104*, 102−112.
(42) Matricardi, C.; Hanske, C.; Garcia-Pomar, J. L.; Langer, J.; Mihi, A.; Liz-Marzán, L. M. Gold nanoparticle plasmonic superlattices as surface-enhanced raman spectroscopy substrates. *ACS Nano* **2018**, *12*, 8531−8539.
(43) Hu, J.; Wang, D.; Bhowmik, D.; Liu, T.; Deng, S.; Knudson, M. P.; Ao, X.; Odom, T. W. Lattice-resonance metalenses for fully reconfigurable imaging. *ACS Nano* **2019**, *13*, 4613−4620.
(44) Olson, J.; Manjavacas, A.; Basu, T.; Huang, D.; Schlather, A. E.; Zheng, B.; Halas, N. J.; Nordlander, P.; Link, S. High chromaticity aluminum plasmonic pixels for active liquid crystal displays. *ACS Nano* **2016**, *10*, 1108−1117.
(45) Kristensen, A.; Yang, J. K. W.; Bozhevolnyi, S. I.; Link, S.; Nordlander, P.; Halas, N. J.; Mortensen, N. A. Plasmonic colour generation. *Nat. Rev. Mater.* **2017**, *2*, 16088.
(46) Esposito, M.; Todisco, F.; Bakhti, S.; Passaseo, A.; Tarantini, I.; Cuscunà, M.; Destouches, N.; Tasco, V. Symmetry breaking in oligomer surface plasmon lattice resonances. *Nano Lett.* **2019**, *19*, 1922−1930.
(47) Czaplicki, R.; Kiviniemi, A.; Laukkanen, J.; Lehtolahti, J.; Kuittinen, M.; Kauranen, M. Surface lattice resonances in second-harmonic generation from metasurfaces. *Opt. Lett.* **2016**, *41*, 2684−2687.
(48) Michaeli, L.; Keren-Zur, S.; Avayu, O.; Suchowski, H.; Ellenbogen, T. Nonlinear surface lattice resonance in plasmonic nanoparticle arrays. *Phys. Rev. Lett.* **2017**, *118*, 243904.
(49) Huttunen, M. J.; Rasekh, P.; Boyd, R. W.; Dolgaleva, K. Using surface lattice resonances to engineer nonlinear optical processes in metal nanoparticle arrays. *Phys. Rev. A* **2018**, *97*, 053817.
(50) Hooper, D. C.; Kuppe, C.; Wang, D.; Wang, W.; Guan, J.; Odom, T. W.; Valev, V. K. Second harmonic spectroscopy of surface lattice resonances. *Nano Lett.* **2019**, *19*, 165−172.
(51) Rodriguez, S. R. K.; Lozano, G.; Verschuuren, M. A.; Gomes, R.; Lambert, K.; De Geyter, B.; Hassinen, A.; Van Thourhout, D.; Hens, Z.; Gomez Rivas, J. Quantum rod emission coupled to plasmonic lattice resonances: A collective directional source of polarized light. *Appl. Phys. Lett.* **2012**, *100*, 111103.
(52) Lozano, G.; Louwers, D. J.; Rodríguez, S. R. K.; Murai, S.; Jansen, O. T. A.; Verschuuren, M. A.; Gómez Rivas, J. Plasmonics for solid-state lighting: enhanced excitation and directional emission of highly efficient light sources. *Light Sci. Appl.* **2013**, *2*, e66.
(53) Zhou, W.; Dridi, M.; Suh, J. Y.; Kim, C. H.; Co, D. T.; Wasielewski, M. R.; Schatz, G. C.; Odom, T. W. Lasing action in strongly coupled plasmonic nanocavity arrays. *Nat. Nanotechnol.* **2013**, *8*, 506−511.
(54) Lozano, G.; Grzela, G.; Verschuuren, M. A.; Ramezani, M.; Gómez Rivas, J. Tailor-made directional emission in nanoimprinted plasmonic-based light-emitting devices. *Nanoscale* **2014**, *6*, 9223−9229.
(55) Schokker, A. H.; Koenderink, A. F. Lasing at the band edges of plasmonic lattices. *Phys. Rev. B* **2014**, *90*, 155452.
(56) Ramezani, M.; Lozano, G.; Verschuuren, M. A.; Gómez-Rivas, J. Modified emission of extended light emitting layers by selective coupling to collective lattice resonances. *Phys. Rev. B* **2016**, *94*, 125406.
(57) Zakharko, Y.; Held, M.; Graf, A.; Rödlmeier, T.; Eckstein, R.; Hernandez-Sosa, G.; Hähnlein, B.; Pezoldt, J.; Zaumseil, J. Surface lattice resonances for enhanced and directional electroluminescence at high current densities. *ACS Photonics* **2016**, *3*, 2225−2230.
(58) Cotrufo, M.; Osorio, C. I.; Koenderink, A. F. Spin-dependent emission from arrays of planar chiral nanoantennas due to lattice and localized plasmon resonances. *ACS Nano* **2016**, *10*, 3389−3397.
(59) Schokker, A. H.; van Riggelen, F.; Hadad, Y.; Alù, A.; Koenderink, A. F. Systematic study of the hybrid plasmonic-photonic band structure underlying lasing action of diffractive plasmon particle lattices. *Phys. Rev. B* **2017**, *95*, 085409.
(60) Wang, D.; Yang, A.; Wang, W.; Hua, Y.; Schaller, R. D.; Schatz, G. C.; Odom, T. W. Band-edge engineering for controlled multi-modal nanolasing in plasmonic superlattices. *Nat. Nanotechnol.* **2017**, *12*, 889.
(61) Guo, R.; Nečada, M.; Hakala, T. K.; Väkeväinen, A. I.; Törmä, P. Lasing at K points of a honeycomb plasmonic lattice. *Phys. Rev. Lett.* **2019**, *122*, 013901.
(62) Vaskin, A.; Kolkowski, R.; Koenderink, F. A.; Staude, I. Light-emitting metasurfaces. *Nanophotonics* **2019**, *8*, 1151.
(63) Yadav, R. K.; Bourgeois, M. R.; Cherqui, C.; Juarez, X. G.; Wang, W.; Odom, T. W.; Schatz, G. C.; Basu, J. K. Room temperature weak-to-strong coupling and the emergence of collective emission from quantum dots coupled to plasmonic arrays. *ACS Nano* **2020**, *14*, 7347−7357.
(64) Yadav, R. K.; Otten, M.; Wang, W.; Cortes, C. L.; Gosztola, D. J.; Wiederrecht, G. P.; Gray, S. K.; Odom, T. W.; Basu, J. K. Strongly coupled exciton-surface lattice resonances engineer long-range energy propagation. *Nano Lett.* **2020**, *20*, 5043−5049.
(65) Yadav, R. K.; Liu, W.; Li, R.; Odom, T. W.; Agarwal, G. S.; Basu, J. K. Room-temperature coupling of single photon emitting quantum dots to localized and delocalized modes in a plasmonic nanocavity array. *ACS Photonics* **2021**, *8*, 576−584.
(66) Boddeti, A. K.; Guan, J.; Sentz, T.; Juarez, X.; Newman, W.; Cortes, C.; Odom, T. W.; Jacob, Z. Long-range dipole-dipole interactions in a plasmonic lattice. *Nano Lett.* **2022**, *22*, 22−28.

https://doi.org/10.1021/acsomega.2c03847
ACS Omega XXXX, XXX, XXX−XXX

(67) Zundel, L.; Cuartero-González, A.; Sanders, S.; Fernández-Domínguez, A. I.; Manjavacas, A. Green tensor analysis of lattice resonances in periodic arrays of nanoparticles. *ACS Photonics* **2022**, *9*, 540−550.
(68) Väkeväinen, A. I.; Moerland, R. J.; Rekola, H. T.; Eskelinen, A.-P.; Martikainen, J.-P.; Kim, D.-H.; Törmä, P. Plasmonic surface lattice resonances at the strong coupling regime. *Nano Lett.* **2014**, *14*, 1721−1727.
(69) Rodriguez, S. R. K.; Feist, J.; Verschuuren, M. A.; Garcia Vidal, F. J.; Gómez Rivas, J. Thermalization and cooling of plasmon-exciton polaritons: towards quantum condensation. *Phys. Rev. Lett.* **2013**, *111*, 166802.
(70) Ramezani, M.; Halpin, A.; Fernández-Domínguez, A. I.; Feist, J.; Rodriguez, S. R.-K.; Garcia-Vidal, F. J.; Gómez Rivas, J. Plasmon-exciton-polariton lasing. *Optica* **2017**, *4*, 31−37.
(71) Hakala, T. K.; Moilanen, A. J.; Väkeväinen, A. I.; Guo, R.; Martikainen, J.-P.; Daskalakis, K. S.; Rekola, H. T.; Julku, A.; Törmä, P. Bose−Einstein condensation in a plasmonic lattice. *Nat. Phys.* **2018**, *14*, 739−744.
(72) Jackson, J. D. *Classical Electrodynamics*; Wiley: New York, 1975.
(73) Novotny, L.; Hecht, B. *Principles of Nano-Optics*; Cambridge University Press: New York, 2006.
(74) Teperik, T. V.; Degiron, A. Design strategies to tailor the narrow plasmon-photonic resonances in arrays of metallic nanoparticles. *Phys. Rev. B* **2012**, *86*, 245425.
(75) Kolkowski, R.; Koenderink, A. F. Lattice resonances in optical metasurfaces with gain and loss. *Proc. IEEE* **2019**, *108* (5), 795−818.
(76) Zundel, L.; Manjavacas, A. Finite-size effects on periodic arrays of nanostructures. *J. Phys.: Photonics* **2019**, *1* (1), 015004.
(77) García de Abajo, F. J. Multiple scattering of radiation in clusters of dielectrics. *Phys. Rev. B* **1999**, *60*, 6086−6102.
(78) Yang, H. U.; D'Archangel, J.; Sundheimer, M. L.; Tucker, E.; Boreman, G. D.; Raschke, M. B. Optical dielectric function of silver. *Phys. Rev. B* **2015**, *91*, 235137.
(79) Rodriguez, S. R. K.; Schaafsma, M. C.; Berrier, A.; Gómez-Rivas, J. Collective resonances in plasmonic crystals: Size matters. *Physica B* **2012**, *407*, 4081−4085.
(80) Zakomirnyi, V. I.; Ershov, A. E.; Gerasimov, V. S.; Karpov, S. V.; Ågren, H.; Rasskazov, I. L. Collective lattice resonances in arrays of dielectric nanoparticles: a matter of size. *Opt. Lett.* **2019**, *44*, 5743−5746.
(81) Kostyukov, A. S.; Rasskazov, I. L.; Gerasimov, V. S.; Polyutov, S. P.; Karpov, S. V.; Ershov, A. E. Multipolar lattice resonances in plasmonic finite-size metasurfaces. *Photonics* **2021**, *8*, 109.
(82) Humphrey, A. D.; Barnes, W. L. Plasmonic surface lattice resonances on arrays of different lattice symmetry. *Phys. Rev. B* **2014**, *90*, 075404.
(83) Lunnemann, P.; Koenderink, A. F. Dispersion of guided modes in two-dimensional split ring lattices. *Phys. Rev. B* **2014**, *90*, 245416.
(84) Li, R.; Bourgeois, M. R.; Cherqui, C.; Guan, J.; Wang, D.; Hu, J.; Schaller, R. D.; Schatz, G. C.; Odom, T. W. Hierarchical hybridization in plasmonic honeycomb lattices. *Nano Lett.* **2019**, *19*, 6435−6441.
(85) Warren, A.; Alkaisi, M. M.; Moore, C. P. Subradiant resonances in Au and Ag bipartite lattices in the visible spectrum. *J. Vac. Sci. Technol.* **2021**, *39*, 063601.
(86) Movsesyan, A.; Besteiro, L. V.; Kong, X.-T.; Wang, Z.; Govorov, A. O. Engineering strongly chiral plasmonic lattices with achiral unit cells for sensing and photodetection. *Adv. Opt. Mater.* **2021**, *10* (14), 2101943.
(87) Ciarella, L.; Tognazzi, A.; Mangini, F.; De Angelis, C.; Pattelli, L.; Frezza, F. Finite-size and illumination conditions effects in all-dielectric metasurfaces. *Electronics* **2022**, *11*, 1017.
(88) Bettles, R. J.; Gardiner, S. A.; Adams, C. S. Enhanced optical cross section via collective coupling of atomic dipoles in a 2D array. *Phys. Rev. Lett.* **2016**, *116*, 103602.
(89) Shahmoon, E.; Wild, D. S.; Lukin, M. D.; Yelin, S. F. Cooperative resonances in light scattering from two-dimensional atomic arrays. *Phys. Rev. Lett.* **2017**, *118*, 113601.
(90) Rui, J.; Wei, D.; Rubio-Abadal, A.; Hollerith, S.; Zeiher, J.; Stamper-Kurn, D. M.; Gross, C.; Bloch, I. A subradiant optical mirror formed by a single structured atomic layer. *Nature* **2020**, *583*, 369−374.

https://doi.org/10.1021/acsomega.2c03847
ACS Omega XXXX, XXX, XXX−XXX

Lattice Resonances Excited by Finite-Width Light Beams

Lauren Zundel,[†,§] Juan R. Deop-Ruano,[‡,§] Rosario Martinez-Herrero,[¶] and Alejandro Manjavacas[*,‡,†]

†*Department of Physics and Astronomy, University of New Mexico, Albuquerque, New Mexico 87106, United States*

‡*Instituto de Óptica (IO-CSIC), Consejo Superior de Investigaciones Científicas, 28006 Madrid, Spain*

¶*Departamento de Óptica, Universidad Complutense de Madrid, 28040 Madrid, Spain*

§*Authors contributed equally to this paper*

E-mail: a.manjavacas@csic.es

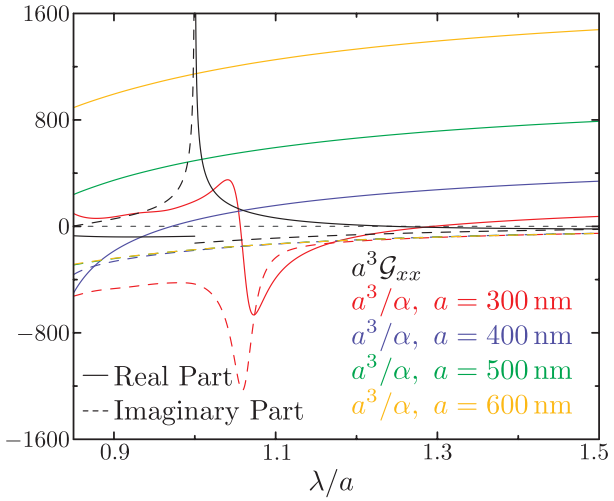

Figure S1: Origin of lattice resonances within the coupled dipole model. The black curves show $a^3\mathcal{G}_{xx}$ for $\mathbf{k}_\parallel = 0$ as a function of λ/a, while the colored curves display a^3/α for different values of a, as indicated by the legend. Note that $a^3\mathcal{G}_{xx}$, when plotted against λ/a, is independent of a. In all cases, the solid curves show the real part of the corresponding quantity, while the dashed curves represent the imaginary part. As discussed in the main paper, the lattice resonance of a periodic array occurs approximately when $\mathrm{Re}\{\alpha^{-1} - \mathcal{G}_{xx}\}$ vanishes. Examining the different curves in the figure, we observe that, in principle, for all of the systems under consideration there is a point at which $\mathrm{Re}\{\mathcal{G}_{xx}\}$ and $\mathrm{Re}\{\alpha^{-1}\}$ cross. However, while for $a = 600\,\mathrm{nm}$ (yellow curves), $a = 500\,\mathrm{nm}$ (green curves), and $a = 400\,\mathrm{nm}$ (blue curves), this crossing point occurs for wavelengths at which $\mathrm{Re}\{\mathcal{G}_{xx}\}$ takes on a significant value, for $a = 300\,\mathrm{nm}$ (red curves), the crossing point occurs at $\lambda/a \approx 1.28$, where $\mathrm{Re}\{\mathcal{G}_{xx}\}$ is practically zero. As a consequence, the resulting resonance corresponds mostly to the localized plasmon of the individual nanoparticles, which appears approximately at the wavelength for which $\mathrm{Re}\{\alpha^{-1}\}$ vanishes. This can also be confirmed by looking at the extinction spectrum of the individual nanoparticles shown in Figure S2. The reader may note additional crossing points for $a = 300\,\mathrm{nm}$, which occur closer to the Rayleigh anomaly, but these do not produce strong features in the extinction spectra due to the large value of $\mathrm{Im}\{\alpha^{-1}\}$ in that region.

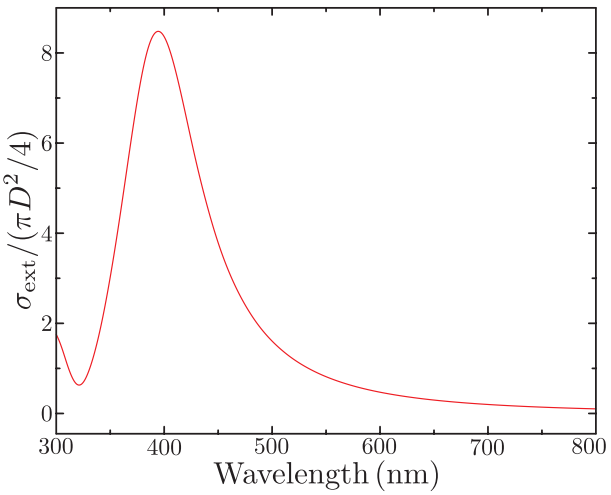

Figure S2: Extinction cross section of an individual silver nanosphere of diameter $D = 100\,\text{nm}$, calculated using the dipole model. The localized plasmon resonance is located at a wavelength of $\lambda \approx 395\,\text{nm}$.

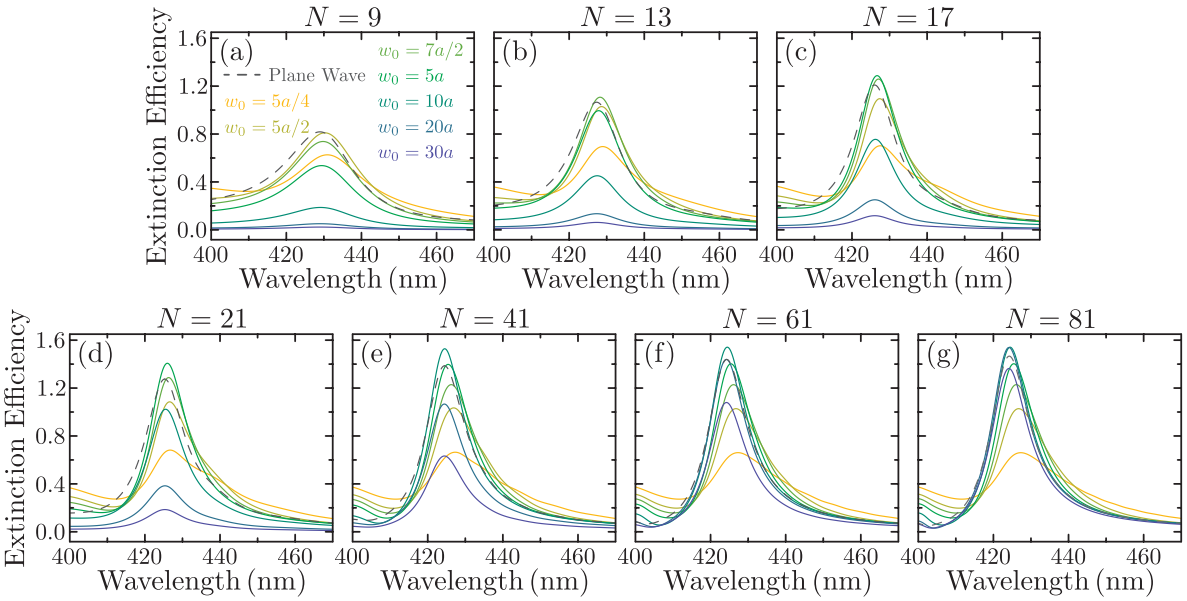

Figure S3: Extinction efficiency spectra for a finite array with $N \times N$ nanoparticles when excited by finite-width light beams, for $N = 9$ (a), $N = 13$ (b), $N = 17$ (c), $N = 21$ (d), $N = 41$ (e), $N = 61$ (f), and $N = 81$ (g). As indicated by the legend, the different colored solid curves correspond to different values of w_0, while the gray dashed curves show the results for the same array when excited by a plane wave. In all cases, the array under consideration has $a = 400\,\text{nm}$ and $D = 100\,\text{nm}$. As discussed in Figure 5 of the main paper, for a given N, there is an optimum value of w_0 that yields the maximum extinction efficiency. Furthermore, this maximum can exceed the value achieved for excitation with a plane wave.